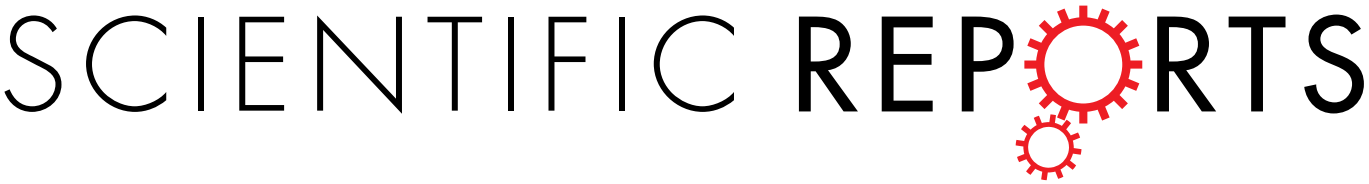

OPEN

Abrupt current switching in graphene bilayer tunnel transistors enabled by van Hove singularities

Received: 26 January 2016
Accepted: 24 March 2016
Published: 21 April 2016

Georgy Alymov[1,2], Vladimir Vyurkov[1,2], Victor Ryzhii[3] & Dmitry Svintsov[1,2]

In a continuous search for the energy-efficient electronic switches, a great attention is focused on tunnel field-effect transistors (TFETs) demonstrating an abrupt dependence of the source-drain current on the gate voltage. Among all TFETs, those based on one-dimensional (1D) semiconductors exhibit the steepest current switching due to the singular density of states near the band edges, though the current in 1D structures is pretty low. In this paper, we propose a TFET based on 2D graphene bilayer which demonstrates a record steep subthreshold slope enabled by van Hove singularities in the density of states near the edges of conduction and valence bands. Our simulations show the accessibility of 3.5×10^4 ON/OFF current ratio with 150 mV gate voltage swing, and a maximum subthreshold slope of $(20\,\mu\text{V/dec})^{-1}$ just above the threshold. The high ON-state current of 0.8 mA/μm is enabled by a narrow (~0.3 eV) extrinsic band gap, while the smallness of the leakage current is due to an all-electrical doping of the source and drain contacts which suppresses the band tailing and trap-assisted tunneling.

The design of field-effect transistors (FETs) operating at sub-0.5 V supply voltage is one of the major challenges for nanoelectronics paving the way to resolve the problem of power dissipation in large integrated circuits. Tunnel FETs (TFETs) with interband tunneling are among the principal candidates to meet this demand[1,2]. The low-voltage switching in TFETs occurs due to a sharp dependence of the tunnel current on the conduction-valence band overlap in a gate-controlled *p-i* or *p-n* junction[3]; once there is no band overlap, there is no tunnel current. This fact, alongside with the smallness of thermionic leakage current and efficient modulation of the barrier transparency by the gate voltage, results in the subthreshold slope of the TFET characteristics surpassing the thermionic limit[4–8] of $(60\,\text{mV/dec})^{-1}$.

It is intuitive that the abrupt variations of electron and hole densities of states (DoS) near the band edges further enhance the switching efficiency of TFETs[9]. For a d-dimensional TFET channel, the DoS scales with energy E above the band edge as $E^{(d-2)/2}$, while the dependence of current J on the gate voltage V_G above the threshold V_T is $J \propto [V_G - V_T]^{(d+1)/2}$ [10,11]. Apart from the density-of-states-enhanced switching, the TFETs with low-dimensional channels demonstrate an improved electrostatic control of the band alignment by the gate voltage[8,12,13]. Theoretically, the effects of DoS on current switching steepness are most pronounced in vertical TFETs based on the two-dimensional crystals[14] and electron-hole bilayers in quantum-confined structures[15,16]. In such TFETs, the joint density of states is nonzero just at one certain value of gate voltage[17] – which could lead to the abrupt-most current switching ever. In practice, the density-of-states effects on the subthreshold steepness are largely smeared. The reason for the smearing in vertical TFETs based on van der Waals heterostructures is the rotational misalignment of 2D layers in momentum space[18]. In common semiconductor structures it is believed that charged defects and dopants lead to pronounced band-tailing and emerging trap-assisted and band-tail tunneling leakage currents[19–21].

In this paper, we theoretically demonstrate that graphene bilayer (GBL) represents an ideal platform for the low-voltage tunnel switches due to its peculiar 'mexican hat' band structure of GBL formed under transverse electric field[22,23] and a van Hove singularity in the DoS right at the bottom of the band edges, as shown in Fig. 1A. The experimental evidence for this singularity were obtained already for graphene samples on disordered SiO_2 substrates: the measurements of infrared absorption[24], quantum capacitance[25], and tunnel current in scanning probe microscope[26] indicated the large density of states. The emergence of high-quality boron nitride substrates

[1]Department of Physical and Quantum Electronics, Moscow Institute of Physics and Technology, Dolgoprudny 141700, Russia. [2]Laboratory of Sub-micron Devices, Institute of Physics and Technology RAS, Moscow 117218, Russia. [3]Research Institute of Electrical Communication, Tohoku University, Sendai 980-8577, Japan. Correspondence and requests for materials should be addressed to D.S. (email: svintcov.da@mipt.ru)

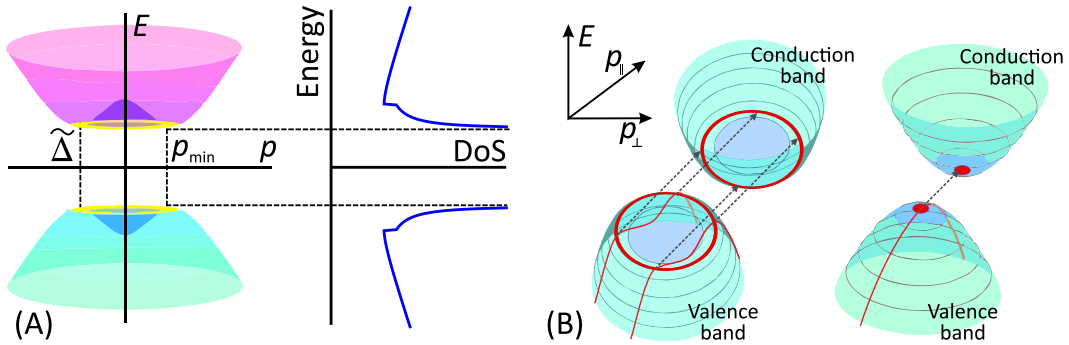

Figure 1. (**A**) Electron spectrum $E(p)$ in graphene bilayer under transverse electric field and the energy dependence of its DoS. The "Mexican hat" feature in the dispersion law leads to the square-root singularities in the DoS near the band edges. Panel (**B**) highlights with red the electron states involved in the interband tunneling at small band overlap in graphene bilayer (left) and in a semiconductor with parabolic bands (right). The phase space for tunneling in graphene bilayer represents a ring, while in a parabolic-band semiconductor it is a point. Dashed lines indicate the tunneling transitions, red lines indicate the trajectories of the tunneling electrons in the valence band.

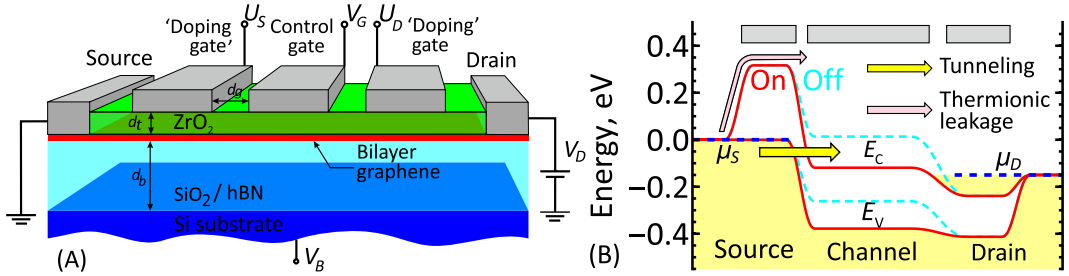

Figure 2. (**A**) Layout of the proposed graphene bilayer TFET with electrically defined source and drain regions (**B**) Band diagram of graphene bilayer TFET for the optimal biasing conditions: $V_B > 0$, $U_S < 0$, $U_D > 0$. At zero top gate bias, $V_G = 0$, the TFET is switched on, while at $V_G < 0$ it is switched off.

for graphene electronic devices started a new chapter in the experimental studies of low-energy spectrum of bilayer, and not only the van Hove singularities[27,28] but even tinier features of carrier spectrum[29] were clearly revealed. In our paper we show that the van Hove singularity results in a steep, linear dependence of the GBL TFET current on the gate voltage above the threshold, which was attributed previously just to the TFETs based on one-dimensional materials[5,8,30–32].

The advantage of graphene bilayer TFETs over those based on 2d materials with parabolic bands in terms of switching steepness can be illustrated by Fig. 2B. As the conduction and valence bands in a GBL tunnel junction overlap, the electrons capable of tunneling are located on a ring in the momentum space. In contrast, the electrons capable of tunneling between simple parabolic bands are located in a small vicinity of an extreme point of the dispersion. Under optimal gate biasing conditions, the proposed TFET demonstrates the current switching over more than 4 orders of magnitude with 150 mV gate voltage swing only. At the same time, the ON-state current density as large as 0.8 mA/μm is accessible due to the low extrinsic band gap of GBL (~0.3 eV) and large DoS far above the band edges.

Although a number of GBL transistors have been proposed[33–35], including the TFETs[36], our structure possesses a unique feature that allows one to exploit the density-of-states effect for tunneling. This feature is electrical doping of source and drain contacts instead of chemical one. This suppresses the band tailing induced by random dopants[37] and minimizes the leakage currents through defect states[38]. Apart from reducing the leakage, this adds the possibility to electrically reconfigure the device between *n*- and *p*-types.

Results

Device structure. The advantages of graphene bilayer for the steep current switching can be fully realized in the structure of the TFET shown schematically in Fig. 2A. A heavily doped silicon substrate acts as a bottom gate used to create the transverse electric field and thus open and manipulate the band gap in GBL[39]. The oxidation of the substrate results in formation of SiO_2 layer playing the role of back gate oxide and substrate for graphene bilayer. Alternatively, the SiO_2 layer can be replaced with hexagonal boron nitride (hBN) possessing a small (~10^{10} cm^{-2}) density of residual charged impurities[40]. A nanometre – thin layer of high-κ dielectric (e.g., zirconium oxide) covers the graphene channel, and the top metal gates are formed above. The side gates near the source and drain contacts induce large densities of holes and electrons, respectively, which also leads to the

formation of an abrupt tunnel junction and energy barriers (see Fig. 2B) for the thermally activated electrons and holes contributing to the OFF-state leakage current.

The operation of a normally open TFET switched off by a negative top gate voltage is illustrated in the band diagram, Fig. 2B. Application of positive voltage to the bottom gate, $V_B > 0$, induces the band gap and provides an excess electron density in bilayer. The p^+ doping of source emerges upon application of negative voltage $U_S < 0$ to the source doping gate. An additional increase in the barrier height for the holes injected from the drain is achieved by applying positive voltage $U_D > 0$ to the drain doping gate. It is instructive that application of high voltage to the doping gates does not result in increased power consumption as this voltage is not changed during the device operation. At zero top gate voltage, the valence band in p^+–source overlaps with the conduction band in the n–type channel, which corresponds to the ON state (red band profiles in Fig. 2B). Upon application of negative voltage to the top gate, the transistor is switched off (dashed blue band profiles in Fig. 2B).

The optimization of the device dimensions aiming at the increase in the ON-state and reduction in the OFF-state currents is quite straightforward: both the effective thickness of the gate dielectric and the distance between the source doping gate and the control gate should be small. These distances are limited just by the possible gate leakage current (see below), we choose them to be $d_t = 2$ nm and $d_g = 5$ nm. The doping gate at the drain is used just to induce high barrier for thermally activated holes; the distance between this gate and the control gate should be large to reduce the transparency of tunnel junction at the drain and get rid of ambipolar leakage.

The fabrication of the device structure in Fig. 2A is technologically feasible with recent advances in the growth of graphene on hBN[41]. The most challenging operation is the formation of the gates at sub-10 nm distance, which is, however, achievable with the combination of self-assembled molecular and electron beam lithographic techniques[42].

Model of the interband tunneling enhanced by van Hove singularities. Our modeling of graphene bilayer TFET relies on a self-consistent determination of the carrier density and band structure[22] followed by the calculation of tunnel current under assumption of ballistic transport (see supplementary material, sections I–III). However, the principal dependence of the tunnel current on the gate voltage can be derived in a very simple fashion. The current is proportional to the number of electrons capable of tunneling between the valence band of source and the conduction band of channel. Once these band overlap by dE in the energy scale, the electrons available for tunneling in graphene bilayer occupy a ring in the momentum space (Fig. 1B, left panel). Their number is proportional to $p_{\min} dE$, where $p_{\min}$ is the momentum corresponding to the bottom of the 'Mexican hat'. One thus concludes that the tunnel current is a linear function of the band overlap which, in turn, is a linear function of the gate voltage. This contrasts with the 2d materials having parabolic bands where the number of electrons available for tunneling is proportional to $\sqrt{E}\,dE$ (Fig. 1B, right panel). As a result, the current in TFETs based on these materials is proportional to the gate voltage raised to the power 3/2.

A rigorous expression for the tunnel current density involves an integral of the single-particle velocity $v_{\|} = dE/dp_{\|}$ timed by the barrier transparency $\mathcal{D}(p_\perp, E)$ and the difference of occupation functions in the valence and conduction bands $f_v(E) - f_c(E)$ over the momentum space $d^2\mathbf{p} = 2dp_\perp dp_{\|}$[10]:

$$J_t = \frac{g_s g_v e}{h^2} \int_{E_c}^{E_v} dE\,[f_v(E) - f_c(E)] \int_0^{p_{\max}(E)} 2dp_\perp \times 2\mathcal{D}(E, p_\perp). \tag{1}$$

Here, $g_s g_v = 4$ is the spin-valley degeneracy factor in graphene, $p_{\max}(E)$ is the maximum transverse momentum of electron at a given energy E, $p_{\max}(E) = \min\{p_c(E), p_v(E)\}$, where $p_c(E)$ and $p_v(E)$ are the inverse functions to the electron dispersion in the conduction and valence bands. The limits of integration over energy are the conduction band edge in the channel, E_c, and the valence band edge in the source, E_v. The factor of two before the quasi-classical barrier transparency comes from the presence of two turning points with zero group velocity in the GBL dispersion at which an electron attempts to tunnel.

The effect of 'Mexican hat' on the current switching steepness can be traced analytically from Eq. 1 by assuming that the conduction band states are empty, valence band states are occupied, and the barrier transparency $\mathcal{D}(E, p_\perp) \approx \mathcal{D}_0$ weakly depends on the energy and transverse momentum. At small band overlap, the momenta of the tunneling electrons in graphene bilayer are close to $p_{\min}$ (Fig. 1B, left panel), which results in

$$J_t \approx 4 g_s g_v \mathcal{D}_0 \frac{e p_{\min}}{h^2} (E_v - E_c). \tag{2}$$

This linear dependence is in agreement with the above qualitative considerations. Previously, such a dependence of the tunnel current on the band overlap was attributed just to the 1D semiconductor structures which proved to be among the best candidates for the TFETs[5,7,43].

An additional increase in the graphene bilayer TFET subthreshold steepness occurs due to the dependence of the transparency $\mathcal{D}(E, p_\perp)$ on the junction field and, hence, gate voltage. The transparency is evaluated by integrating the imaginary part of the electron momentum inside the band gap, which results in (see Supporting information, section III)

$$\mathcal{D}(E, p_\perp) \approx \exp\left[-\frac{\pi l}{2\hbar} \operatorname{Im} p_{\|}(E = 0)\right], \tag{3}$$

where $\operatorname{Im} p_{\|}(E = 0)$ is the imaginary part of electron momentum evaluated at the midgap, and l is the length of the classically forbidden region (tunneling path length). The latter is given by $l = \tilde{\Delta}/eF$ for $p_\perp < p_{\min}$, and $l = 2E(p_\perp)/eF$ for $p_\perp > p_{\min}$, where F is the electric field at the junction found from the solution of Poisson's

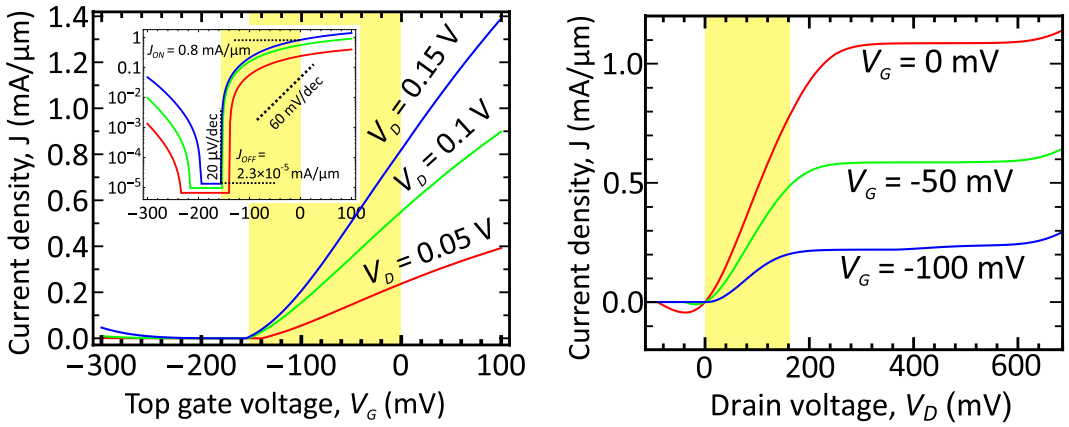

Figure 3. Calculated room-temperature gate transfer (left) and current-voltage (right) characteristics of graphene bilayer TFET at fixed bias voltages at auxiliary gates: $V_B = 3.3$ V, $U_S = -0.6$ V, $U_D = 0.25$ V. Top gate dielectric is 2 nm ZrO_2, $\kappa = 25$, back gate dielectric is 10 nm SiO_2, spacing between the source doping and control gates $d_g = 5$ nm, spacing between drain doping and control gates is 10 nm. The regions highlighted in yellow correspond to the drive voltage swing of 150 mV, in which sufficient ON/OFF ratio and high ON-state current are achieved. Inset: gate transfer characteristic in the log scale.

equation, and $\tilde{\Delta}$ is the band gap in the GBL. The thermionic leakage currents were evaluated with equations similar to (1) by setting the unity transmission probability and constraining the energy integral to the particles with the energies above the barrier.

Characteristics of the graphene bilayer TFET. The calculated room-temperature $J(V_G)$–characteristics of graphene bilayer TFET at different drain bias V_D are shown in Fig. 3A. The current density just above the threshold voltage is a linear function of V_G, in agreement with the simple density-of-states arguments and Eq. (2). With increasing the top gate voltage, the slope of $J(V_G)$-curve slightly increases due to the sensitivity of the tunnel barrier transparency to the junction field. The subthreshold slope at $V_G = V_{th}$ reaches $(20\,\mu\text{V/dec})^{-1}$ and is limited by the small thermionic current $J_{th} \simeq 1.3 \times 10^{-5}$ mA/μm and the gate leakage current $J_g \simeq 1.0 \times 10^{-5}$ mA/μm. About 100 mV below the threshold, the ambipolar leakage at the drain tunnel junction becomes pronounced; this can be, however, minimized by placing the drain doping gate at large distance from the control gate.

The drain characteristics of graphene bilayer TFET shown in Fig. 3B demonstrate a pronounced current saturation typically absent in single graphene layer FETs. This saturation is due to the limited energy range in which the tunneling injection is possible. At very high drain bias ~600 mV, the barrier for thermally activated holes at drain junction is sufficiently lowered, which leads to the further increase in current. At negative drain bias, the transistor current can be viewed as that of $p^+ - n^+$ tunnel diode between source and channel. The emerging negative differential resistance is due to the dependence of the band edges in the channel on the amount of injected carriers: at high electron density, the bands in the channel are lifted upwards, which reduces the source-channel band overlap and switches the tunneling off.

For low-power applications, the maximization of the highest subthreshold slope is not as important as minimization of the supply voltage V_S required to switch the transistor between the ON- and OFF-states. Considering the current at $V_G = 0$ V as the ON-state current ($J_{ON} = 0.8$ mA/μm in Fig. 3B at $V_D = 0.15$ V), and the leakage current as the OFF-state current ($J_{ON}/J_{OFF} = 3.5 \times 10^4$), we have obtained $V_S = 150$ mV. In a conventional MOSFET, the gate voltage swing $V_S \geq 285$ mV is required to achieve the same current switching ratio. The average subthreshold slope of our TFET over 4.5 decades of current is 33 $(\text{mV/dec})^{-1}$. With this characteristic, it outperforms all sub-thermal tunnel switches[2] based on silicon[4], germanium[6], III-V hetero junctions[5], and carbon nanotubes[7] reported to date. Only recently a vertical TFET based on MoS_2/germanium junction with a similar value of the average subthrehold slope was demonstrated[44], however, its ON-state current density of 1 μA/μm leaves much to be desired.

The aggregate quality of the TFET, accounting for both average subthreshold slope and current density, can be characterized by an I_{60}–figure of merit[45] which is the current density at the point where the subthreshold slope equals $(60\,\text{mV/dec})^{-1}$. While the best I_{60} reported to date equals 6 nA/μm (InAs nanowire/Si heterojunction TFET[5]), in our TFET structure $I_{60} = 150\,\mu$A/μm.

The unique characteristics of GBL TFET surpassing the existing TFETs are enabled by the three factors. First of all, it is the small extrinsic band gap (for doping gate voltages used in Fig. 3, $\tilde{\Delta} \approx 0.3$ eV) that guarantees elevated tunneling probability ($\mathcal{D}$~0.1) and large current density. It is remarkable that there exists a lower limit of the interband transparency in GBL due to the saturation of the band gap $\tilde{\Delta}$ at high transverse field, $\mathcal{D} \geq \exp\{-\pi\gamma_1^2/4e\hbar F v_0\}$, where $\gamma_1 \approx 0.4$ eV is the interlayer hopping integral and $v_0 \approx 10^6$ m/s is the band velocity. Such transparency is sufficient to reach appreciable ON/OFF ratio, and it still enables pronounced ON-state current. At the same time, most semiconducting monolayers have large intrinsic band gaps (1.9 eV for MoS_2, 1.3 eV for WS_2, etc.), while in the 2D structures based on III–V materials being narrow-gap in the bulk, the gap value increases significantly due to the quantum confinement[46]. Secondly, the singular DoS near the band edges

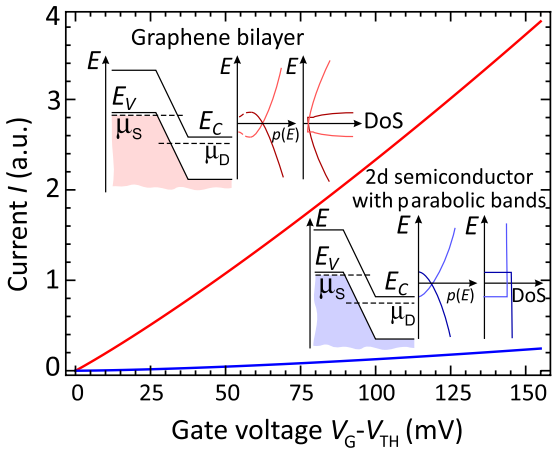

Figure 4. Comparison of the gate transfer characteristics of GBL TFET and a TFET based on an equivalent 2D semiconductor with the same barrier transparency D_0, but with different (parabolic) band structure. Numerical values of the effective masses are taken for bulk InAs. The insets show the band diagrams overlaid with electron-hole spectra and the energy dependence of DoS.

allows an abrupt switching of tunnel current. Even if there existed a parabolic-band 2D material with the same band gap and the same barrier transparency in the TFET structure, its current density would be given by (see supplemental material, section IV)

$$J_{t,\mathrm{par}} \approx \frac{4g_s}{3}\frac{e}{h^2}\mathcal{D}_0\sqrt{\frac{2m_c m_v}{m_c+m_v}}(E_v-E_c)^{3/2}, \tag{4}$$

where m_c and m_v are the conduction and valence band effective masses and, similar to the derivation of Eq. (2), we have assumed the barrier transparency $\mathcal{D}_0$ to be energy- and momentum independent. Last but not least, it is large density of states in GBL growing linearly at *high* energies that contributes to the high ON-state current. The numerical comparison of current density in graphene bilayer and its equivalent parabolic band counterpart is presented in Fig. 4 for the effective mass values typical for narrow-gap III–V semiconductors ($m_c = 0.024m_0$, $m_v = 0.026m_0$ for InAs). At 150 mV gate voltage above the threshold, the current density in graphene bilayer exceeds 15 times that in a parabolic-band material. The factor of two is due to the valley degeneracy absent in III-V's, another factor of two is due to the tunneling at two turning points of the 'Mexican hat' dispersion, and the remainder of 3.5 is due to the finiteness of electron momentum at the edge of the 'Mexican hat'.

Gate leakage and band tailing: the insulator selection rules. The steep switching of the tunnel current by the gate voltage can be masked by the leakage to the gates, band-tail and trap-assisted tunneling[19–21]. The latter factors might have masked the onset of the interband current in the recent measurements of graphene bilayer tunnel junctions[38,47]. A careful selection of the gate dielectrics providing high interface quality is required to minimize these effects.

The main reason for the band tailing comes from the fluctuations of electric potential produced by the random charged defects or dopants[37]. This effect is most pronounced in the TFETs with source and drain intentionally doped chemically. In the TFETs with electrically doped contacts, only residual charged impurities inevitably present in the substrate contribute to the band tailing. To provide a quantitative view on the band tailing in graphene bilayer on different substrates, we have evaluated the quasi-classical DoS $\rho(E)$ in the presence of fluctuating potential by integrating the singular 'bare' DoS ρ_0 over the probabilities of voltage fluctuations[37]

$$\rho(E) = \frac{1}{\sqrt{2\pi\langle V^2\rangle}}\int_{-\infty}^{+\infty}\rho_0(E-eV)\exp\left(-\frac{V^2}{2\langle V^2\rangle}\right)dV, \tag{5}$$

where $\langle V^2\rangle$ is the root-mean-square amplitude of the voltage fluctuations proportional to the impurity density n_i. The calculated energy dependencies of the 'smeared' DoS are shown in Fig. 5. For the parameters of chemical doping used in the pioneering proposal of the GBL TFET[36], $n_i = 4\times10^{13}\,\mathrm{cm}^{-2}$, the conduction and valence bands almost merge together, which would result in a poor OFF-state, nothing to say about high switching steepness. A slight peak in the DoS near the band bottom becomes noticeable already at impurity density of $5\times10^{12}\,\mathrm{cm}^{-2}$ which corresponds to the low-quality graphene on SiO_2 substrates. In graphene samples on a high-quality SiO_2[48], the smearing of the band edge is order of 10 meV. The ultimate band abruptness of ~5 meV can be achieved in graphene samples encapsulated in boron nitride, providing the residual impurity density of $\sim5\times10^{10}\,\mathrm{cm}^{-2}$ [40]. At this limit, the fluctuation-induced smearing of the bands becomes negligible, and the behavior of the DoS near the bottom of the "Mexican hat" is governed by the trigonal warping distortions of electron spectrum due to the next-nearest neighbor interactions[22]. Using the exact spectrum of GBL with trigonal warping, we estimate the

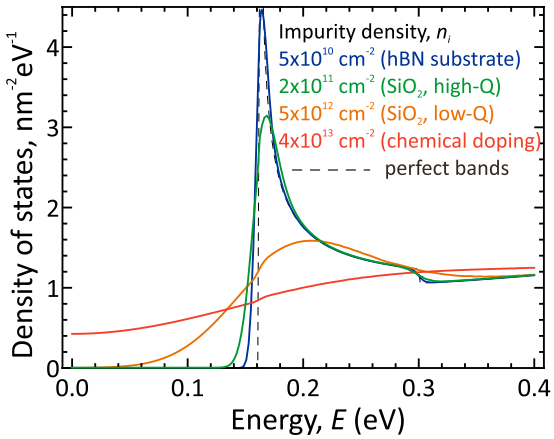

Figure 5. Calculated energy dependencies of the DoS in the conduction band of graphene bilayer at different densities of charged impurities (corresponding to the substrates of different quality). The electron density is held fixed at $4 \times 10^{13}\,\mathrm{cm}^{-2}$, the nominal energy gap is 0.3 eV.

energy scale where the trigonal warping is relevant as $\delta\varepsilon \approx 20$ meV. Already for relatively small gate voltages, $V_G - V_{th} > \delta\varepsilon/e$, these corrections are irrelevant and the linearity of the $J(V_G)$–characteristic holds.

The gate leakage may also limit the minimum achievable OFF-state current, while at the same time small effective gate oxide thickness is required to efficiently control the band structure in the channel by the gate voltage. Among the common high-κ materials, zirconium oxide ($\kappa \approx 25$) looks as an optimal solution for the GBL TEFT due to the large band offset with respect to graphene ($U_b = 2.9$ eV[49]) and elevated tunneling mass $m_t \approx 0.3 m_0$[50]. We have evaluated the leakage current from graphene with electron (hole) density of $n_{e(h)}$ into the metal gate to be (see Supporting information, section VI)

$$J_g = 8eL_g n_{e(h)} \frac{U_b}{\hbar} \frac{k_F l_{\mathrm{loc}}}{1 + (k_F l_{\mathrm{loc}})^2} \mathcal{D}_g, \tag{6}$$

where $l_{\mathrm{loc}} = \hbar/\sqrt{2m_t U_b}$ is the electron localization length in the direction perpendicular to the graphene bilayer, k_F is the Fermi wave vector in the metal, $\mathcal{D}_g$ is the transparency of the barrier separating GBL and the gate, and L_G is the gate length. Under the biasing conditions of Fig. 3, the gate leakage current is estimated to be $J_t = 1.0 \times 10^{-5}\,\mathrm{mA}/\mu\mathrm{m}$ which is below the thermionic leakage level (in this estimate, we have taken $L_g = 20$ nm and $k_F = 2\,\text{Å}^{-1}$).

Discussion

We have proposed and substantiated the operation of a graphene bilayer TFET exploiting the van Hove singularities in the density of states near the band edges. The presence of these singularities leads to the increased steepness of the gate characteristics and to the high ON-state current as well. The subthreshold slope of $J(V_G)$ curve in the proposed FET reaches the maximum of $(20\,\mu\mathrm{V/dec})^{-1}$, while only 150 mV gate voltage swing is required to change the current density from $J_{ON} \approx 1\,\mathrm{mA}/\mu\mathrm{m}$ down to $J_{OFF} \approx 2 \times 10^{-5}\,\mathrm{mA}/\mu\mathrm{m}$. As a matter of fact, the effects of singular DoS on the interband tunneling are possible just in the TFET structures with an all-electrical doping, where the effects of band tailing and trap-assisted tunneling are minimized.

Such steep switching in the lateral TFETs based on 2d materials is possible if only the van Hove singularities are present both at the top of the valence and the bottom of the conduction band. This property is unique to the graphene bilayer and is absent in other 2d materials (e.g., those based on III–V compounds), where a 'Mexican hat' structure is formed in one of the bands due to the spin-orbit coupling[51]. We can thus conclude that graphene bilayer is an only two-dimensional material where the switching of interband tunnel current is as steep as in one-dimensional semiconductors, whereas the large on-state current is inherited from the single layer graphene.

At present, it is challenging to quantitatively compare the results our model to the experimental data, which are limited to the characteristics of graphene bilayer Esaki-type $p^+ - n^+$ tunnel junctions[38]. Our theory predicts a linear growth of diode current at small forward voltages, and a linear decrease in current at voltages $eV \leqslant \xi_n + \xi_p$, where ξ_n and ξ_p are the electron and hole Fermi energies in the n^+ and p^+-doped regions (see Fig. 6, blue lines). This behavior qualitatively agrees with the experimentally observed $I(V)$-curves. It is worth noting that a widely used phenomenological model of tunneling proposed by Esaki[52], where the current is proportional to the integral of states' densities in conduction and valence bands timed by the difference of occupation functions, predicts a different $I(V)$-curve. In such model, the current reaches its maximum at $eV = \xi_n + \xi_p$ and then drops abruptly (Fig. 6, red lines). Such $I(V)$ curves are not observed in the experiments, which speaks in favor of our rigorous model of tunneling.

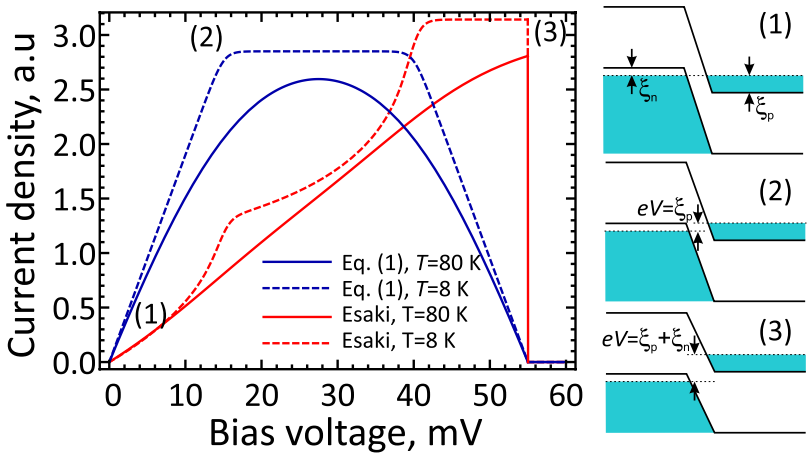

Figure 6. Characteristics of graphene bilayer $p^+ - n^+$ tunnel diodes calculated with our model, Eq. 1, blue lines, and with Esaki model[52], red line. The temperature of 80 K corresponds to the experimental data obtained in ref. 38, $\xi_n = 40$ meV, $\xi_p = 15$ meV. The band diagrams correspond to the characteristic points (1), (2), and (3) of the $I(V)$-curve. In Esaki model, the current is proportional to the product of states densities and the difference of occupation functions integrated over the band overlap. The current calculated with Esaki model reaches its maximum as the van Hove singularities in the conduction and valence bands overlap, and then drops abruptly to zero. Such highly asymmetric peaks in tunnel current have never been observed in experiment[38], which speaks in favor of our tunneling model.

Methods

The modeling of GBL TFET is based on the self-consistent determination of carrier density and band structure under fixed gate voltages[22] followed by the calculation of tunnel current with Eq. (1). The necessity for self-consistent calculation is dictated by the dependence of the energy gap on the electric field between graphene layers comprising the GBL; the field, in turn, depends on the induced carrier density which is sensitive to the band structure. The distribution of electric field at the tunneling junction required for the evaluation of the barrier transparency is calculated with the conformal mapping technique. The numerical model is described in detail in Supporting information, sections I-II. In section III of the Supporting information, an approximate analytic model of GBL TFET is presented.

The effect of charged impurities present in the substrate on the singular density of states in graphene bilayer is evaluated with Kane's quasi-classical model of band tails[37]. The revision of the model for the two-dimensional GBL is presented in Supporting information, section V.

The gate leakage current is estimated with a quantum-mechanical model of graphene bilayer tunnel coupled to the continuum of delocalized states in the metal gate. The model is presented in Supporting information, section VI.

References

1. Ionescu, A. M. & Riel, H. Tunnel field-effect transistors as energy-efficient electronic switches. *Nature* **479,** 329–337 (2011).
2. Lu, H. & Seabaugh, A. Tunnel field-effect transistors: State-of-the-art. *IEEE Journal of the Electron Devices Society* **2,** 44–49 (2014).
3. Seabaugh, A. C. & Zhang, Q. Low-voltage tunnel transistors for beyond CMOS logic. *Proc. of the IEEE* **98,** 2095–2110 (2010).
4. Choi, W. Y., Park, B.-G., Lee, J. D. & Liu, T.-J. K. Tunneling field-effect transistors (TFETs) with subthreshold swing (SS) less than 60 mV/dec. *IEEE El. Dev. Lett.* **28,** 743–745 (2007).
5. Tomioka, K., Yoshimura, M. & Fukui, T. Sub 60 mV/decade switch using an InAs nanowire-Si heterojunction and turn-on voltage shift with a pulsed doping technique. *Nano Lett.* **13,** 5822–5826 (2013).
6. Krishnamohan, T., Kim, D., Raghunathan, S. & Saraswat, K. Double-gate strained-Ge heterostructure tunneling FET (TFET) with record high drive currents and ≪60mV/dec subthreshold slope. In *IEDM 2008 IEEE International Electron Devices Meeting*, 1–3, doi: 10.1109/IEDM.2008.4796839 (2008).
7. Appenzeller, J., Lin, Y.-M., Knoch, J. & Avouris, P. Band-to-band tunneling in carbon nanotube field-effect transistors. *Phys. Rev. Lett.* **93,** 196805 (2004).
8. Hanna, A. N., Fahad, H. M. & Hussain, M. M. InAs/Si hetero-junction nanotube tunnel transistors. *Sci. Rep.* **5,** 9843, doi: 10.1038/srep09843 (2015).
9. Agarwal, S. & Yablonovitch, E. Using dimensionality to achieve a sharp tunneling FET turn-on. In *69th Annual Device Research Conference (DRC)*, 199–200, doi: 10.1109/DRC.2011.5994496 (2011).
10. Kane, E. O. Theory of tunneling. *J. Appl. Phys.* **32,** 83–91 (1961).
11. Keldysh, L. Behavior of non-metallic crystals in strong electric fields. *Sov. Phys. JETP* **6,** 763 (1958).
12. Knoch, J., Mantl, S. & Appenzeller, J. Impact of the dimensionality on the performance of tunneling FETs: Bulk versus one-dimensional devices. *Solid-State Electron.* **51,** 572–578 (2007).
13. Fahad, H. & Hussain, M. High-performance silicon nanotube tunneling fet for ultralow-power logic applications. *IEEE Trans. EL. Dev.* **60,** 1034–1039 (2013).
14. Britnell, L. *et al.* Resonant tunnelling and negative differential conductance in graphene transistors. *Nature Communications* **4,** 1794 (2013).
15. Lattanzio, L., De Michielis, L. & Ionescu, A. M. The electron-hole bilayer tunnel FET. *Solid-State Electron.* **74,** 85–90 (2012).
16. Agarwal, S., Teherani, J. T., Hoyt, J. L., Antoniadis, D. A. & Yablonovitch, E. Engineering the electron-hole bilayer tunneling field-effect transistor. *IEEE Trans. El. Dev.* **61,** 1599–1606 (2014).

17. Zhao, P., Feenstra, R., Gu, G. & Jena, D. SymFET: A proposed symmetric graphene tunneling field-effect transistor. *IEEE Trans. El. Dev*. **60,** 951–957 (2013).
18. Mishchenko, A. *et al.* Twist-controlled resonant tunnelling in graphene/boron nitride/graphene heterostructures. *Nat. Nanotechnol*. **9,** 808–813 (2014).
19. Vandooren, A. *et al.* Analysis of trap-assisted tunneling in vertical Si homo-junction and SiGe hetero-junction tunnel-FETs. *Solid-State Electron*. **83,** 50–55 (2013).
20. Bessire, C. D. *et al.* Trap-assisted tunneling in Si-InAs nanowire heterojunction tunnel diodes. *Nano Lett*. **11,** 4195–4199 (2011).
21. Khayer, M. A. & Lake, R. K. Effects of band-tails on the subthreshold characteristics of nanowire band-to-band tunneling transistors. *J. Appl. Phys*. **110,** 074508 (2011).
22. McCann, E., Abergel, D. S. & Fal'ko, V. I. The low energy electronic band structure of bilayer graphene. *Eur. Phys. J-Spec. Top.* **148,** 91–103 (2007).
23. Zhang, Y. *et al.* Direct observation of a widely tunable bandgap in bilayer graphene. *Nature* **459,** 820–823 (2009).
24. Kuzmenko, A. B. *et al.* Infrared spectroscopy of electronic bands in bilayer graphene. *Phys. Rev. B* **79,** 115441 (2009).
25. Young, A. F. *et al.* Electronic compressibility of layer-polarized bilayer graphene. *Phys. Rev. B* **85,** 235458 (2012).
26. Brar, V. W. *et al.* Scanning tunneling spectroscopy of inhomogeneous electronic structure in monolayer and bilayer graphene on SiC. *Appl. Phys. Lett.* **91,** 122102 (2007).
27. Kim, K. *et al.* Van der Waals heterostructures with high accuracy rotational alignment. *Nano Letters* **16,** 1989–1995 (2016).
28. de la Barrera, S. C. & Feenstra, R. M. Theory of resonant tunneling in bilayer-graphene/hexagonal-boron-nitride heterostructures. *Appl. Phys. Lett.* **106,** 093115 (2015).
29. Varlet, A. *et al.* Anomalous sequence of quantum hall liquids revealing a tunable Lifshitz transition in bilayer graphene. *Phys. Rev. Lett.* **113,** 116602 (2014).
30. Björk, M. T., Knoch, J., Schmid, H., Riel, H. & Riess, W. Silicon nanowire tunneling field-effect transistors. *Appl. Phys. Lett.* **92,** 193504 (2008).
31. Zhang, Q., Fang, T., Xing, H., Seabaugh, A. & Jena, D. Graphene nanoribbon tunnel transistors. *IEEE El. Dev. Lett.* **29,** 1344–1346 (2008).
32. Jena, D. A theory for the high-field current-carrying capacity of one-dimensional semiconductors. *J. Appl. Phys* **105,** 123701 (2009).
33. Ryzhii, V., Ryzhii, M., Satou, A., Otsuji, T. & Kirova, N. Device model for graphene bilayer field-effect transistor. *J. Appl. Phys.* **105,** 104510 (2009).
34. Fiori, G. & Iannaccone, G. On the possibility of tunable-gap bilayer graphene FET. *IEEE El. Dev. Lett*. **30,** 261–264 (2009).
35. Svintsov, D., Vyurkov, V., Ryzhii, V. & Otsuji, T. Effect of mexican hat on graphene bilayer field-effect transistor characteristics. *Jpn. J. Appl. Phys.* **50,** 070112 (2011).
36. Fiori, G. & Iannaccone, G. Ultralow-voltage bilayer graphene tunnel FET. *IEEE El. Dev. Lett*. **30,** 1096–1098 (2009).
37. Kane, E. O. Thomas-Fermi approach to impure semiconductor band structure. *Phys. Rev*. **131,** 79–88 (1963).
38. Miyazaki, H. *et al.* Observation of tunneling current in semiconducting graphene *p-n* junctions. *J. Phys. Soc. Jap*. **81,** 014708 (2012).
39. Zhang, Y. *et al.* Direct observation of a widely tunable bandgap in bilayer graphene. *Nature* **459,** 820–823 (2009).
40. Kretinin, A. V. *et al.* Electronic properties of graphene encapsulated with different two-dimensional atomic crystals. *Nano Lett.* **14,** 3270–3276 (2014).
41. Liu, Z. *et al.* Direct growth of graphene/hexagonal boron nitride stacked layers. *Nano Lett.* **11,** 2032–2037 (2011).
42. Negishi, R. *et al.* Fabrication of nanoscale gaps using a combination of self-assembled molecular and electron beam lithographic techniques. *Appl. Phys. Lett*. **88,** 223111 (2006).
43. Hwang, W. S. *et al.* Transport properties of graphene nanoribbon transistors on chemical-vapor-deposition grown wafer-scale graphene. *Appl. Phys. Lett.* **100,** 203107 (2012).
44. Sarkar, D. *et al.* A subthermionic tunnel field-effect transistor with an atomically thin channel. *Nature* **526,** 91–95 (2015).
45. Vandenberghe, W. G. *et al.* Figure of merit for and identification of sub-60 mV/decade devices. *Appl. Phys. Lett.* **102,** 013510 (2013).
46. Jena, D. Tunneling transistors based on graphene and 2-d crystals. *Proc. of the IEEE* **101,** 1585–1602 (2013).
47. Aparecido-Ferreira, A. *et al.* Enhanced current-rectification in bilayer graphene with an electrically tuned sloped bandgap. *Nanoscale* **4,** 7842–7846 (2012).
48. Tan, Y.-W. *et al.* Measurement of scattering rate and minimum conductivity in graphene. *Phys. Rev. Lett.* **99,** 246803 (2007).
49. Zheng, W. *et al.* Electronic structure differences in ZrO_2 vs HfO_2. *J. Phys. Chem. A* **109,** 11521–11525 (2005).
50. Clima, S. *et al.* Determination of ultimate leakage through rutile TiO_2 and tetragonal ZrO_2 from ab initio complex band calculations. *IEEE El. Dev. Lett*. **34,** 402–404 (2013).
51. Ganichev, S. D. & Golub, L. E. Interplay of Rashba/Dresselhaus spin splittings probed by photogalvanic spectroscopy – a review. *Phys. Status Solidi (b)* **251,** 1801–1823 (2014).
52. Esaki, L. New phenomenon in narrow germanium $p - n$ junctions. *Phys. Rev*. **109,** 603–604 (1958).

Acknowledgements

The work was supported by the Russian Scientific Foundation (Project #14-29-00277) and by the Russian Foundation for Basic Research (Grant #14-07-00937). The work at RIEC was supported by the Japan Society for Promotion of Science (Grant-in-Aid for Specially Promoted Research #23000008).

Author Contributions

D.S. conceived the idea of tunnel current switching enhanced by the van Hove singularities in graphene bilayer, G.A. developed the model of interband tunneling and calculated the transistor characteristics. V.V. and V.R. proposed the device structure. G.A. and D.S. wrote the manuscript. All authors reviewed the manuscript.

Additional Information

Supplementary information accompanies this paper at http://www.nature.com/srep

Competing financial interests: The authors declare no competing financial interests.

How to cite this article: Alymov, G. *et al.* Abrupt current switching in graphene bilayer tunnel transistors enabled by van Hove singularities. *Sci. Rep.* **6**, 24654; doi: 10.1038/srep24654 (2016).